Eur. Phys. J. B **68**, 293–308 (2009)
DOI: 10.1140/epjb/e2008-00374-7

THE EUROPEAN PHYSICAL JOURNAL B

Regular Article

# Spin 3/2 fermions with attractive interactions in a one-dimensional optical lattice: phase diagrams, entanglement entropy, and the effect of the trap

G. Roux[1,a], S. Capponi[2], P. Lecheminant[3], and P. Azaria[4]

[1] Institute for Theoretical Physics C, RWTH Aachen University, 52056 Aachen, Germany
[2] Laboratoire de Physique Théorique - IRSAMC, UPS and CNRS, Université de Toulouse 31062 Toulouse, France
[3] Laboratoire de Physique Théorique et Modélisation, Université de Cergy-Pontoise, CNRS, 95302 Cergy-Pontoise, France
[4] Laboratoire de Physique Théorique de la Matière Condensée, Université Pierre et Marie Curie, CNRS, 75005 Paris, France

Received 3 July 2008
Published online 27 September 2008 – 

**Abstract.** We study spin 3/2 fermionic cold atoms with attractive interactions confined in a one-dimensional optical lattice. Using numerical techniques, we determine the phase diagram for a generic density. For the chosen parameters, one-particle excitations are gapped and the phase diagram is separated into two regions: one where the two-particle excitation gap is zero, and one where it is finite. In the first region, the two-body pairing fluctuations (BCS) compete with the density ones. In the other one, a molecular superfluid (MS) phase, in which bound-states of four particles form, competes with the density fluctuations. The properties of the transition line between these two regions is studied through the behavior of the entanglement entropy. The physical features of the various phases, comprising leading correlations, Friedel oscillations, and excitation spectra, are presented. To make the connection with experiments, the effect of a harmonic trap is taken into account. In particular, we emphasize the conditions under which the appealing MS phase can be realized, and how the phases could be probed by using the density profiles and the associated structure factor. Lastly, the consequences on the flux quantization of the different nature of the pairing in the BCS and MS phases are studied in a situation where the condensate is in a ring geometry.

**PACS.** 03.75.Mn Multicomponent condensates; spinor condensates – 71.10.Pm Fermions in reduced dimensions (anyons, composite fermions, Luttinger liquid, etc.) – 71.10.Fd Lattice fermion models (Hubbard model, etc.)

## 1 Introduction

Recent experimental progress achieved in trapped ultracold atomic gases provides a great opportunity for exploring the physics of strong correlations in clean systems, thanks to the tunability of interactions using optical lattices and Feshbach resonance. A large number of interesting phenomena of condensed matter physics and nuclear physics is then expected to be accessible in the context of ultracold atomic gases [1]. A prominent example is the observation of the Mott insulator-superfluid quantum phase transition with cold bosonic atoms in an optical lattice [2], and its possible fermionic analogue, the Mott insulator-metallic phase transition, recently investigated in a two-component Fermi gas [3]. A second breakthrough is the trapping of a two-component Fermi gas and the study of the crossover from fermionic superfluidity of Cooper (BCS) pairs to Bose-Einstein condensation of tightly bounded molecules [4–6].

The superfluid behavior of multicomponent Fermi gases with more than two hyperfine states might also lead to interesting properties that have been explored recently [7–31]. In particular, the interplay between superfluidity and magnetism, which stems from the presence of the different internal states, can be investigated. Experimentally, three component Fermi gases can be created by trapping the three lowest hyperfine states of $^6$Li atoms in a magnetic field, or by considering $^{40}$K atoms. In addition, the magnetic field dependence of the three scattering lengths of $^6$Li is known experimentally and can be tuned via Feshbach resonance [32] which opens for the experimental realization of a three-component fermionic lattice model. In fact, such a degenerate Fermi gas has been realized experimentally very recently [33], and a four-component Fermi gas could also be achieved using $^{40}$K atoms [34].

The existence of these internal degrees of freedom is expected to give rise to some exotic superfluid phases. In this respect, a molecular superfluid (MS) phase might be

[a] e-mail: roux@physik.rwth-aachen.de

stabilized where more than two fermions form a bound state. Such a state might be relevant to several topics in physics. For instance, the quark model of nuclear matter at low density describes nucleons as three-fermion bound states. Such a trionic phase has been found in one-dimensional integrable fermionic model with three colors [7] and its emergence in the context of three-component ultracold fermions has been discussed recently [22,26,27,29,30]. The possibility that superfluidity is sustained by a condensate based on four-fermion bound states (quartet) might be also explored in cold atomic physics [11,14–16,26,31]. Such a superfluid behavior has already been found in very different contexts such as nuclear physics for instance, where a four-particle condensate – the $\alpha$ particle – is known to be favored over deuteron condensation at low densities [35,36]. Such a quartet condensation can also occur in semiconductors with the formation of biexcitons [37]. A quartetting phase, which stems from the pairing of Cooper pairs, has also been found in a model of one-dimensional (1D) Josephson junctions [38] and in four-leg Hubbard ladders [39].

In this paper, we will investigate the low-energy properties of (hyperfine) spin-3/2 (i.e. four-component) fermionic cold atoms confined in a one-dimensional optical lattice in light of the possible formation of a quartetting phase. Due to Pauli's principle, low-energy $s$-wave scattering processes of spin 3/2 fermionic atoms are allowed in the singlet and quintet channels, so that the effective Hamiltonian with contact interactions reads [10,40]

$$\mathcal{H} = -t \sum_{i,\alpha} [c^\dagger_{\alpha,i} c_{\alpha,i+1} + \text{h.c.}] - \sum_i \mu_i \, n_i + U_0 \sum_i P^\dagger_{00,i} P_{00,i} + U_2 \sum_{i,m} P^\dagger_{2m,i} P_{2m,i}, \quad (1)$$

where $c^\dagger_{\alpha,i}$ is the fermionic creation operator at site $i$, in one of the $\alpha = \pm 1/2, \pm 3/2$ hyperfine states. The on-site density operator is denoted by $n_i = \sum_\alpha c^\dagger_{\alpha,i} c_{\alpha,i}$. The chemical potential $\mu_i$ can be uniform (called $\mu$ for grand-canonical Quantum Monte-Carlo calculations), inhomogeneous in presence of the trap, zero for DMRG calculation (canonical ensemble). For convenience, the lattice spacing is set to unity. Singlet and quintet operators in equation (1) are defined using Clebsch-Gordan coefficients

$$P^\dagger_{Jm,i} = \sum_{\alpha\beta} \langle Jm|\alpha\beta\rangle c^\dagger_{\alpha,i} c^\dagger_{\beta,i}.$$

For instance, the spin 3/2 on-site singlet operator reads $P^\dagger_{00,i} = P^\dagger_i = c^\dagger_{3/2,i} c^\dagger_{-3/2,i} - c^\dagger_{1/2,i} c^\dagger_{-1/2,i}$. A convenient way to rewrite the Hamiltonian is to express it in terms of the density and singlet pairing operators:

$$\mathcal{H} = -t \sum_{i,\alpha} [c^\dagger_{\alpha,i} c_{\alpha,i+1} + \text{h.c.}] - \sum_i \mu_i \, n_i + \frac{U}{2} \sum_i n_i^2 + V \sum_i P^\dagger_i P_i, \quad (2)$$

with $U = 2U_2$ and $V = U_0 - U_2$. This model has an exact SO(5) symmetry [41,42], and, for the fine-tuning $U_0 = U_2$ (or $V = 0$), a SU(4) symmetry. In the latter case, the Hamiltonian reduces to a Hubbard-like Hamiltonian with only on-site density-density interactions. It resembles the usual SU(2) Hubbard model, but with four colors instead of two and we refer to it in the following as the SU(4) line. Similarly, we refer to the $U = 0$ and $V < 0$ line as the BCS line since the singlet pairing is naturally favored in this regime. The model (2) has essentially three physical parameters: the density of particles $n$, and the two interactions $U/t$ and $V/t$ in units of the hopping $t$ (set to one in the following). Experimentally, the interacting parameters can be varied by tuning the scattering lengths (for instance to negative values) and the depth of the optical lattice [4].

In the homogeneous situation (i.e. in absence of the harmonic trap), the phase diagram of model (2) at zero temperature has been investigated by means of low-energy approaches [14,15,31] and numerical calculations [26,43] such as the density-matrix renormalization group (DMRG) technique [44–46] and Quantum Monte-Carlo (QMC) simulations [47–49]. Away from half-filling, there are two very different spin-gapped phases which are separated by an Ising quantum phase transition. In the first one, for instance along the SU(4) line with $U < 0$, the BCS singlet-pairing instability is suppressed. The leading instability is an atomic-density wave (ADW) with wave-vector $2k_F$ ($k_F$ being the Fermi wave-vector) or a quartetting one. In particular, at sufficiently low-density, a dominant MS instability emerges which marks the onset of the quartetting phase. In the second spin-gapped phase, basically obtained along the BCS line, the $2k_F$-ADW instability has now a short-range behavior and BCS singlet pairing competes with a molecular density-wave (MDW) with a $4k_F$ wave-vector.

In this paper, we give more details on the large-scale numerical calculations which have been used in the short papers [26,43] and bring several new results. In this respect, we present the phase diagram of model (2) in absence of the trap for a generic filling which is not one atom per site as in reference [43]. Moreover, the Friedel oscillations and excitation spectra are studied, together with the quantum phase transition between the two spin-gapped phases from the behavior of the entanglement entropy. We also introduce a simple observable, the molecules fraction, which could be useful for experiments. Then, we investigate the inhomogeneous situation and the effet of a harmonic confining potential on the quartetting phase in order to make contact with future experiments in spinor fermion ultracold gases. Finally, the nature of the flux quantization in the BSC and MS phases is analyzed in a ring geometry.

The paper is organized as follows. In Section 2, we recall the main results obtained within the low-energy approach and we describe the technical details of the three numerical methods used in this work. Section 3 presents our main results concerning the phase diagram and the physical properties of the phases of model (2) in

**Table 1.** The possible phases, obtained by means of the low-energy approach, of spin-3/2 cold atoms with attractive interactions; the symbol exp. denotes a correlation with an exponential decay and the other correlations have a power-law behavior; $N_{2k_F}(x)$ (respectively $N_{4k_F}(x)$) corresponds to the $2k_F$ (respectively $4k_F$) part of the density correlation function.

| | Phases | | | |
|---|---|---|---|---|
| | ADW ($K<2$) MS ($K>2$) | | BCS ($K>1/2$) MDW ($K<1/2$) | |
| Correlator | exponent | wave-vector | exponent | wave-vector |
| $Q(x)$ | $2/K$ | 0 | $2/K$ | 0 |
| $P(x)$ | exp. | 0 | $1/(2K)$ | 0 |
| $N_{2k_F}(x)$ | $K/2$ | $2k_F$ | exp. | $2k_F$ |
| $N_{4k_F}(x)$ | $2K$ | $4k_F$ | $2K$ | $4k_F$ |

the homogeneous situation. The experimental signatures of the quartetting phase are then discussed in Section 4 which includes, in particular, the effect of the trap. Finally, our concluding remarks are summarized in Section 5.

## 2 Low-energy and numerical approaches

### 2.1 Low-energy approach

In this section, we recall the main results of the low-energy approach [14,15,31,50] on the behavior of the different order parameters that identify the possible phases of model (2). For a generic density, the low-energy Hamiltonian separates into two commuting pieces: a density and (hyperfine) spin part. This result is nothing but the famous "spin-charge" separation which is the hallmark of 1D incommensurate electronic systems [51,52]. The $U(1)$ density fluctuations remain gapless while the spin part is fully gapped for parameters with either $U$ or $V$ negative. In the terminology of 1D electronic systems, we have the stabilization of a Luther-Emery liquid phase [51,52]. However, in contrast with the standard $F=1/2$ (i.e. two-component) fermions, two very different Luther-Emery liquid phases emerge here, which are separated by an Ising quantum phase transition when $U=V<0$ in the weak-coupling limit.

In the first one (dubbed ADW/MS region), a representative being the SU(4) line with $U<0$, the BCS singlet pairing with order parameter $P_i$ displays a short-range behavior. The leading instability of this region corresponds to the order parameter which has the slowest (power-law) decaying correlations at zero temperature. The natural candidates in this first phase are the density correlation $N(x)=\langle n_i n_{i+x}\rangle$ and the quartet correlation $Q(x)=\langle Q_i Q_{i+x}^\dagger\rangle$ with $Q_i=c_{3/2,i}c_{-3/2,i}c_{1/2,i}c_{-1/2,i}$. The latter instability is rather natural since when $U<0$ and $V=0$, the density-density term in equation (2) has a tendency to form on-site molecules (the quartets) made of four particles in all different hyperfine states. The leading asymptotic behavior of these correlations can be computed within the low-energy approach and the results are summarized in Table 1. The power-law decay of these correlation functions depends only on the Luttinger parameter $K$ which is a non-universal function of the interaction parameters and the density $n$. A perturbative estimate, valid in the weak-coupling regime $|V|/t, |U|/t \ll 1$, gives

$$K = 1/\sqrt{1+[V+3U]/\pi v_F}, \tag{3}$$

with the Fermi velocity $v_F = 2t\sin(\pi n/4)$. Within the same approximation, the sound velocity of the gapless density mode reads:

$$u = v_F\sqrt{1+[V+3U]/\pi v_F}. \tag{4}$$

For non-interacting fermions, we have $K=1$ and $u=v_F$. From equation (3), we see that attractive interactions increase the Luttinger parameter and that an artificial divergence, which occurs when the denominator vanishes, signals the breakdown of the perturbative calculation. From Table 1, we deduce that the leading instability is the $2k_F(=\pi n/2)$ ADW one for $K<2$, whereas the quartetting MS phase is stabilized when $K>2$. In the latter regime, we have an exotic Luther-Emery liquid with a confinement of pairs (that would be objects with charge $2e$ in a context of charged particles) and the emergence of quartets (similarly, objects with a $4e$ charge). A related Luther-Emery phase has been found in a totally different context corresponding to the formation of multi-magnon bound-states in the spin-1/2 $J_1$–$J_2$ Heisenberg chain under magnetic field [53]. Inside the ADW/MS region, there is no sharp quantum phase transition and only a smooth crossover. In this respect, it might be interesting to observe that there is a continuity between weak and strong coupling regimes in this region. Indeed, the higher-harmonics in the quartet correlation can be estimated by means of the low-energy approach:

$$\begin{aligned} Q(x) \sim\ & A\,x^{-2/K} + B\cos(2k_F x)\,x^{-(2/K+K/2)} \\ & + C\cos(4k_F x)\,x^{-2(K+1/K)}, \end{aligned} \tag{5}$$

$A, B, C$ being non-universal amplitudes. On the other hand, along the SU(4) line at small densities and strong attractive $U$, the physics is essentially governed by hard-core bosons $b_i \sim Q_i$ with repulsive interactions. The bosonic correlation function of this model is known from the harmonic-fluid approach [54,55]:

$$\begin{aligned} \langle b_i b_{i+x}^\dagger\rangle \sim\ & A\,x^{-1/2K_b} + B\cos(2\pi\rho_0 x)\,x^{-(1/2K_b+2K_b)} \\ & + C\cos(4\pi\rho_0 x)\,x^{-(8K_b+1/2K_b)}, \end{aligned} \tag{6}$$

where $\rho_0 \simeq n/4$ is the density of the bosons and $K_b$ is the underlying Luttinger parameter. From equations (5) and (6), we thus observe that there is a continuity between weak and strong coupling regimes with $K=4K_b$. In particular, we also deduce an upper bound for the Luttinger parameter $K$: $K_{\max}=4$ since the value $K_b=1$ for non-interacting hard-core bosons [54,55] is expected in the limit of vanishing densities.

In the second spin-gapped region (called in the following BCS/MDW region), obtained for instance along the BCS line, the pairing term in equations (2) stabilizes the order parameter $P_i$ of the Cooper pairs. Now,

the $2k_F$ ADW instability is a strongly fluctuating order since the $2k_F$ part of the density correlation has an exponential decay. As seen in Table 1, the competing orders in this phase are the BCS instability with equal-time correlations $P(x) = \langle P_i P^\dagger_{i+x}\rangle$ and $4k_F(=\pi n)$ ADW operator. A BCS phase is stabilized for $K > 1/2$ which is analogue to the standard Luther-Emery phase of spin-1/2 electrons [51,52]. For $K < 1/2$, a MDW phase, which is characterized by a $4k_F$ oscillation of the density fluctuations, is predicted to emerge. For a generic filling, we expect no quantum phase transition between BCS and MDW phases but a smooth crossover. For the commensurate filling of one atom per site ($n = 1$), we have shown in reference [43] that a Mott transition occurs and that the MDW phase is replaced by a Mott-insulating phase with bond ordering.

In summary, we observe that the nature of the phases found within the low-energy approach are governed by the non-universal Luttinger parameter $K$ which is a function of the density $n$ and the interactions $U/t, V/t$. It is thus crucial to have a reliable evaluation of $K$. Since model (2) is not integrable in the generic case, numerical calculations of this parameter are required.

### 2.2 Numerical methods

We use three different numerical methods to investigate the phase diagram of model (2): mainly the density-matrix renormalization group (DMRG), but also the exact diagonalization (ED) and quantum Monte-Carlo (QMC) techniques.

DMRG calculations were performed at zero temperature with open boundary conditions (OBC) using an *exact* mapping of model (2) onto a two-leg SU(2) Hubbard ladder model with special couplings (here, the spin index can take only two values $\sigma = \pm 1/2$):

$$\mathcal{H}^{\mathsf{L}} = -t^{\mathsf{L}}_{\parallel} \sum_{i,\beta,\sigma} [c^\dagger_{i+1,\beta,\sigma} c_{i,\beta,\sigma} + \text{h.c.}] + U^{\mathsf{L}} \sum_{i,\beta} n_{i,\beta,\uparrow} n_{i,\beta,\downarrow} + V^{\mathsf{L}}_{\perp} \sum_i n_{i,1} n_{i,2} + J^{\mathsf{L}}_{\perp} \sum_i \mathbf{S}_{i,1} \mathbf{S}_{i,2}. \quad (7)$$

We use $\mathsf{L}$ as the label for the ladder couplings, and $\perp$ for couplings between the two chains and $\parallel$ for couplings along the chains. $\beta = 1, 2$ is the chain index, $n_{i,\beta,\sigma} = c^\dagger_{i,\beta,\sigma} c_{i,\beta,\sigma}$, $\mathbf{S}_{i,\beta}$ is the spin operator, and $n_{i,\beta} = \sum_\sigma n_{i,\beta,\sigma}$ the local density. For the hoppings, we have $t^{\mathsf{L}}_{\parallel} = t$ and $t^{\mathsf{L}}_{\perp} = 0$. For the on-site interaction, $U^{\mathsf{L}} = U$. For the next-nearest neighbor density-density interaction on rungs, $V^{\mathsf{L}}_{\perp} = U + V/2$, and also a Heisenberg coupling on the rungs $J^{\mathsf{L}}_{\perp} = -2V$. All other couplings are equal to zero. In this mapping, the local number of states per site is strongly reduced as it is $2^2 = 4$ for a SU(2) Hubbard site and $2^4 = 16$ for a spin-3/2 Hubbard site. Symmetries are used to fix the total number of fermions to $N_f$ and the total $z$-component of the spin to zero. We have typically kept 1000 states of the reduced density matrix, and sometimes up to 1400. Convergence depends on the regions of the phase diagram, and is harder with the trap. On the SU(4) line with large $|U|$, the convergence is very good as the physics is essentially the one of hard-core bosons. The discarded weight typically ranges from $10^{-11}$–$10^{-8}$ when both interactions are negative (and not to small) to $10^{-6}$ if one is positive or small. Moreover, the discarded weight decreases with density so that simulations become easier and more accurate in this regime.

On the SU(4) line with total $S^z = 0$, the numbers of particles $N_\sigma$ per specie are independently conserved. Therefore, with an appropriate choice of boundary conditions and $N_\sigma$ (for instance periodic boundary conditions and $N_\sigma$ odd), the particles do not experience any statistics so that, by means of a Jordan-Wigner transformation, the model is *strictly equivalent* to a hard-core boson model on a *four*-leg ladder for which chains are only coupled via a density-density interaction term $V^{\mathsf{L}}_{\perp} = U$ between all chains. Such a bosonic model has no sign problem and can be efficiently simulated by QMC techniques such as the Stochastic Series Expansion (SSE) algorithm [47,48]. We use the ALPS software implementation of the SSE algorithm [56,57]. Note that, contrarily to DMRG, the algorithm works in the grand-canonical ensemble and at finite temperature. Away from the SU(4) line, Fermi statistics cannot be avoided and therefore, we have also used a determinantal QMC algorithm (DQMC), which has no sign problem over a relatively wide range of parameters [43]. For this algorithm, we have used the projector approach that provides ground-state properties with a fixed number of particles [49].

## 3 Phase diagram

This section gathers results on the phase diagram for a generic density, i.e. a density for which no commensurability effects are expected, and which is sufficiently low to realize the MS phase on the SU(4) line [26]. We choose $n = 0.75$. We first explain how the Luttinger parameter $K$ is computed numerically, before giving more details on the physics of each phase.

### 3.1 Extracting the Luttinger exponent

As one can see from Table 1, the Luttinger exponent $K$ can be extracted from algebraically decaying correlation functions. For instance, the quartet (or MS) correlations $Q(x)$ gives access to $2/K$ in all regions of the phase diagram. They can be reliably computed with DMRG if the number of state kept is sufficiently large. As data are computed on finite and open chains, there is no translational invariance and all correlators depend on both positions of the sites. For instance, $Q(x) = \langle Q_i Q^\dagger_{i+x}\rangle$ will actually depend on $i$. We fix $i = m = L/2$ to be at the middle of the chain and control finite size effects using results from conformal theory [55]. By denoting the conformal distance $d(x|L) = L|\sin(\pi x/L)|/\pi$, the leading term of the quartet

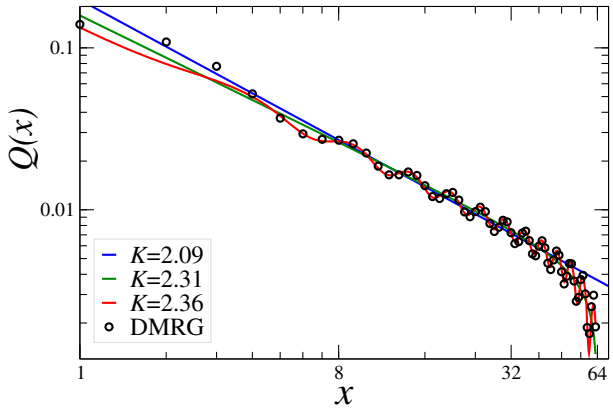


**Fig. 1.** Typical fit of the quartet correlations in the MS phase on the SU(4) line. Data are obtained by DMRG with $L = 128$ and $U/t = -4$ at filling $n = 0.75$. See text for the three fitting functions. Using equation (8) gives the Luttinger parameter $K = 2.36$.

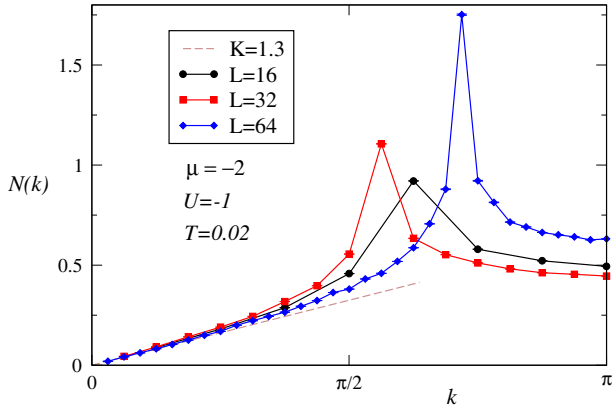


**Fig. 2.** Density structure factor $N(k)$ obtained from QMC SSE simulations at low temperature ($T = 0.02t$), fixed chemical potential $\mu = -2t$ and for various sizes $L$. Since finite-size effects are rather small, an accurate estimate of $K$ can already be obtained on small systems from the small-$k$ linear behavior. Here, for $U/t = -1$ and a density close from 1.2, one gets $K \simeq 1.3$ which is compatible with the DMRG estimate.

correlations is of the bosonic form

$$Q(x) = \rho_0 \sqrt{1 + c_0 \frac{\cos(\pi n x/2 + \delta)}{[d(2(m-x)|2L)]^{K/4}}} \times \left[ \frac{\sqrt{d(2x|2L)d(2m|2L)}}{d(x+m|2L)d(x-m|2L)} \right]^{2/K}. \quad (8)$$

If one writes the $Q_i$ operator in a density-phase representation $\sqrt{q_i} e^{i\phi(x_i)}$, the first term is $\sqrt{q_i q_{i+x}}$ where $q_i = \langle Q_i^\dagger Q_i \rangle$ denotes the local density of quartets (bosons). Because of OBC, Friedel oscillations appear close to the edge, leading to a typical $2k_F$ cosine term that decays algebraically *from* the edge (see a discussion in Sect. 3.6). In terms of bosons, this decay of the density fluctuations [55] is controlled by $K_b$ which gives $K/4$ for quartets. Note that the scaling dimension of the density operator is also $K/4$. Thus, our fitting procedure stems more from the phenomenology of hard-core bosons than from an exact result. Note that oscillations cannot be explained by the harmonics of the quartetting correlations as derived in equation (5) because the exponents of the sub-leading terms are of order 2 and 5, which are far too large to explain the oscillations (which actually increase with $x$). The amplitude $c_0$ and phase-shift $\delta$ are unknown parameters. The second term is the leading algebraic decaying term $x^{-2/K}$ modified by finite size effects. The function replacing $1/x$ in between the brackets accounts for the vanishing of the wave-function at the edge of the box which induces a drop in the correlations. Typical data in the MS phase are given in Figure 1 for a chain with size $L = 128$. Rather strong Friedel oscillations are observed in the signal (in the BCS phase, these oscillations are much smaller). Three fits are used to extract $K$. Firstly, a simple algebraic fit (which corresponds to taking $c_0 = 0$ and $L = \infty$ in Eq. (8)) yields $K = 2.09$. Secondly, a fit without the $2k_F$ oscillations ($c_0 = 0$) gives $K = 2.31$. Thirdly, a fit using equation (8) with $\rho_0$, $c_0$, $\delta$ and $K$ as free parameters gives $K = 2.36$ and an excellent agreement with the data. It is thus important to take into account the finite size effects to have a reliable evaluation of $K$. In a previous work [43], we have used an averaging of the correlators over $i$; this suppresses the oscillations but gives a less accurate estimate for $K$. A similar fit function as in equation (8) but with a phenomenologically introduced cosine oscillations was used in reference [26] and leads to results very close to the ones obtained from equation (8).

Another systematic way of calculating the Luttinger exponent is to use the density correlations $N(x)$ and the associated structure factor $N(k)$, where $k$ is the wave-vector. This method is particularly suited for QMC as the density operator can be more easily sampled than the quartet operator. The value of $K$ is extracted from the small wave-vector behavior of $N(k)$:

$$K = \frac{2\pi}{4} \lim_{k \to 0} \frac{N(k)}{k}, \quad (9)$$

with a factor 4 in the denominator corresponding to the number of fermionic flavors. For instance, this procedure has been shown to be very accurate for the spin-1/2 Hubbard model [58]. An example of a typical fit is given in Figure 2 at fixed chemical potential $\mu$. Note that, since the QMC SSE algorithm is grand canonical, the density will slightly vary when the parameters (temperature or size) are changed[1]. This effect can be seen from the position of the $2k_F = \pi n/2$ peak in Figure 2. One advantage is that a linear fit is simple to perform. However, in the limit of small densities, the $2k_F$ peak approaches 0 which makes it difficult to find the linear small-$k$ regime on finite size systems.

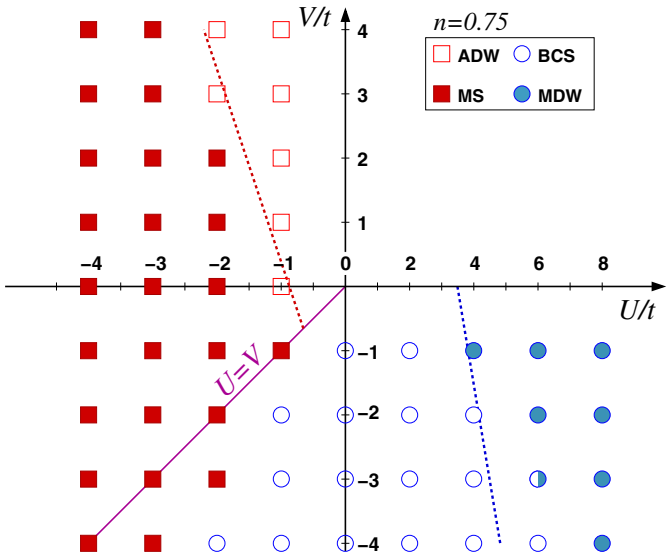


**Fig. 3.** Phase diagram of the spin-3/2 Hubbard model (2) at the incommensurate filling $n = 0.75$, and for attractive interactions ($U \leq 0$ or $V \leq 0$) from DMRG calculations (see text for definitions of the phases). The $U = V$ line is the perturbative estimate for the transition between the two regions BCS/MDW and the ADW/MS regime. The dashed lines are the perturbative estimates for the crossovers between respectively BCS/MDW and ADW/MS.

### 3.2 Phase diagram at the generic density n = 0.75

Figure 3 displays the phase diagram of the spin-3/2 Hubbard model for attractive interactions ($U \leq 0$ or $V \leq 0$) and a density $n = 0.75$. The density is chosen in such a way that the MS exists (from Ref. [26] we know that this is the case on the SU(4) line), and that there are no commensurate phases[2] (in contrast to $n = 1$ [15,43] or $n = 2$). Note that the MS phase is not accessible at filling $n = 1$ while the perturbative estimate of equation (3) predicts its existence [43]. From its wide extension in Figure 3, we observe that the MS phase, is very robust under the symmetry breaking term $V$. Thus, the quartet molecular phase is not an artifact of the SU(4) symmetry. This is an important result since in most of the realistic situations, the actual symmetry is expected to be smaller than SU(4). Part of the answer is given in 1D systems by the accepted view that, at sufficiently low energies and for generic interactions, the dynamical symmetry is most likely to be enlarged [59]: though the SU(4) symmetry is not an exact symmetry, it is physically meaningful as an effective low-energy theory. As a consequence, the SU(4) model studied in reference [26] is a very good starting point to explore the main features of the quartet phase.

As a remark, we argue that the quartet phase also emerges in a problem with no extended SO(5) symmetry. For instance, we can consider the two-leg ladder model described in Sect. 2.2 on the SU(4) line. The model simplifies to a model of two spin-1/2 Hubbard chains coupled only by the inter-chain density-density interaction $V_\perp^\parallel$. If we relax the constraint $V_\perp^\parallel = U$ and let $V_\perp$ vary, we have the following picture. For $V_\perp = 0$, the SU(2) Hubbard chains are exactly solvable by the Bethe-ansatz technique and the corresponding Luttinger parameters $u_{SU(2)}, K_{SU(2)}$ can be computed exactly [60]. Bosonizing the $V_\perp$ coupling between the two chains gives, for the symmetric combination of the modes, the Luttinger parameter

$$K_+ = K_{SU(2)} / \sqrt{1 + V_\perp K_{SU(2)} / \pi u_{SU(2)}}. \qquad (10)$$

$K_+$ can be identified with $K$ when $V_\perp = U$ and governs the quartetting correlations as in equation (5). We see that a negative $V_\perp$ gives $K_+ > K_{SU(2)}$. Yet, we know from reference [60] that $K_{SU(2)} \to 2$ in the limit of low densities and negative $U_{SU(2)}$. A finite negative $V_\perp$ should thus easily stabilize a superfluid quartet phase with $K_+ > 2$. Furthermore, we must note that equation (10) is perturbative in $V_\perp$ but otherwise valid for *arbitrary* values of $u_{SU(2)}$ and $K_{SU(2)}$, which are known even in the strong coupling regime $|U_{SU(2)}|/t \gg 1$. In particular, the fact that $K$ saturates along the $U/t$ line of the SU(4) Hubbard model [26] might be similar to the saturation of $K_{SU(2)}$ at large $|U_{SU(2)}|$. For both models, the saturation is associated with the onset of a hard-core boson regime of pairs for SU(2), and quartets for SU(4). A similar superfluid phase where pairing of bosons along the rungs occurs in the bosonic ladder model [61], the phenomenology and perturbative argument being essentially the same.

### 3.3 Excitations gaps and spectra

We now turn to the excitation gaps in the two regions of the phase diagram. In the context of cold atoms experiments, the quartet phase can be probed by radio-frequency spectroscopy to measure the excitation gaps of the successive quartet dissociation process. In particular, the existence of molecules can be characterized by finite one and two particle gaps while four particle excitations remain gapless. This feature alone does not distinguish between various phases (dominant superfluid or density correlations) but it allows to check for the formation of bound-states.

The energy gap to fill when adding $p$ particles in the system is defined by

$$\Delta_{pp} = E_0(N_f + p) + E_0(N_f + p) - 2E_0(N_f), \qquad (11)$$

with $E_0(N_f)$ the energy of the ground-state with $N_f$ particles. We choose $N_f = 4(2m + 1)$, with $m$ an integer, so that we would have closed shells in the case of periodic boundary conditions. Figure 4 provides the results on the

[1] Note that canonical algorithms are also available for such models.

[2] Actually, one could argue that $n = 3/4$ is a simple fraction and that commensurate phases can occur. However, in terms of bosons, this would correspond to a density 3/16 for which a Luttinger exponent $K_b = 2/16^2$ is required to drive the transition [52], giving $K = 1/32$ which is very small, but could, in principle, still appear at very large interactions.

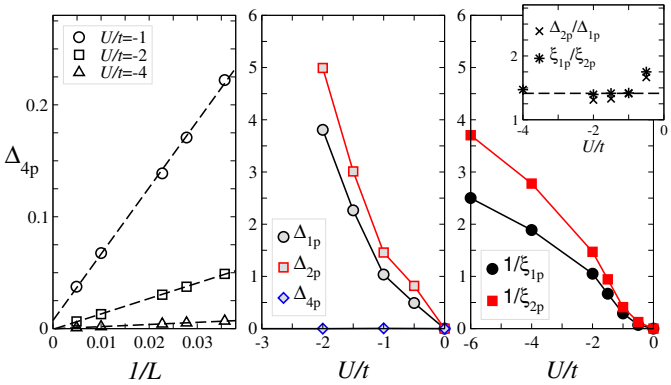


**Fig. 4.** One, two and four particle gaps along the SU(4) line for the density $n = 1$. *Left:* scaling of the four particles gap for different $U$. *Middle:* $\Delta_{1p}$ and $\Delta_{2p}$ as a function of $U/t$ on a finite system with $L = 12$, and extrapolated $\Delta_{4p}$. *Right:* we also show the inverse of the correlation lengths $\xi_{1p,2p}$ obtained from the Green's function and the pairing correlations. *Inset:* comparison of the numerically obtained ratios and the $\sqrt{2}$ prediction.

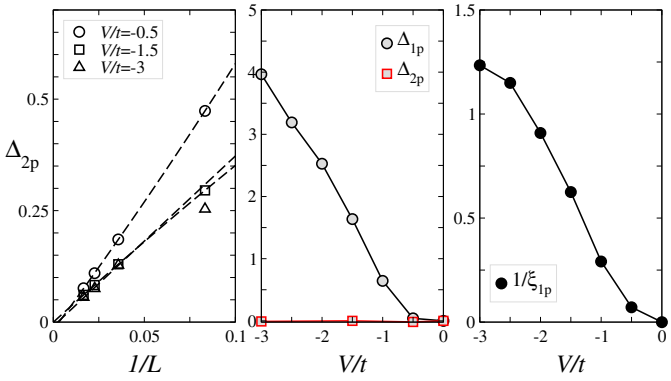


**Fig. 5.** One and two particle gaps along the BCS line for the density $n = 1$. *Left:* scaling of $\Delta_{2p}$. *Middle:* $\Delta_{1p}$ on a finite system with $L = 12$, and extrapolated $\Delta_{2p}$. *Right:* the inverse correlation length of the Green's function $\xi_{1p}$ is also shown.

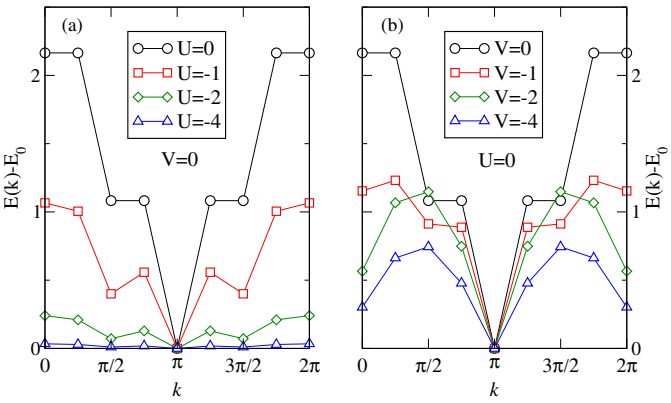


**Fig. 6.** Lowest energy $E(k)$ as a function of the momentum $k$ for a ring of length $L = 8$ with 8 fermions for various interactions (a) along the SU(4) line ($V = 0$); (b) along the BCS line ($U = 0$). Antiperiodic boundary conditions are chosen to have closed shells. Energies are measured relative to the ground-state energy.

one, two and four particles gaps on the SU(4) line with a density $n = 1$ and a small system $L = 12$. For large sizes and interaction $|U|$, quartets are strongly bound and convergence of systems with $N_f$ not a multiple of four can fail. Indeed, even after many sweeps, the density distributions are not symmetrical with respect to the center of the chain. Results given in Figure 4 are those with symmetrical ground-states and well-converged energies. The small size of the chain may cause finite size effects but, still, a clear opening of the one and two particle gaps is found. For $\Delta_{4p}$, no convergence issues are found and scaling can be performed. Figure 4 shows that $\Delta_{4p} = 0$ in the thermodynamical limit, in agreement with the algebraic decay of the correlations. To further check the consistency of the numerics and the low-energy theory, we use the fact that the ratio $\Delta_{2p}/\Delta_{1p}$ is known to be exactly $\sqrt{2}$ from the integrability of the SU(4) Thirring model [62] describing the spin part of the Hamiltonian in the low-energy approach. This ratio is plotted for the $L = 12$ gaps in the inset of Figure 4 and agrees reasonably well with the prediction.

Another way of probing the presence of finite gaps is to look at the associated correlation functions. The one and two particles gaps, when finite, are associated with the exponential decay of the Green's and pairing correlation functions, as observed in reference [43]. In this case, the two correlation lengths behave as $\xi_{1p,2p} \sim u/\Delta_{1p,2p}$, where $u$ is the sound velocity of the bosonic mode. The inverse correlation lengths are given as a function of interaction in Figure 4. The same universal ratio is expected for the correlation length and well observed numerically on Figure 4. These results support the correctness of the low-energy approach, even for strong couplings, and in particular the validity of the separation of the spin-charge sectors.

Similarly, gaps and the inverse correlation length can be computed by DMRG on the BCS line. Results are given in Figure 5 which shows a smooth opening as soon as interactions are turned on. Two and four particle excitations are gapless while a one-particle gap opens. We only show $\Delta_{2p}$ because $\Delta_{4p}$ also scales to zero when $\Delta_{2p} = 0$ in the thermodynamical limit. These behaviors follow the results obtained in reference [43] for the pairing and correlation functions. To give additional insights on the opening of the one-particle gap, we provide the evolution of the inverse correlation length of the Green's function $\xi_{1p}$. Experimentally, the one-particle correlation length $\xi_{1p}$ will appear in the momentum distribution of the condensate.

Exact diagonalization on small systems on a ring allows for the computation of the excitation energy spectrum $E(k)$ vs. momentum $k$. Even if finite size effects can be important, some qualitative information can be extracted. Figure 6 displays the spectra along the SU(4) and BCS lines for the density $n = 1$. Note that anti-periodic boundary conditions are used to have closed shells when $U = V = 0$ for a chain with $4(2m)$ fermions with $m$ an integer. On the SU(4) line, we observe that the $2k_F$ excitation has a lower energy than the $4k_F$, which is associated with the dominant density fluctuations at $2k_F$

in this region of parameters. As $|U|$ increases, all energies go down, so the sound velocity of the charge mode $u$ also decreases, in agreement with the perturbative estimate of equation (4). The spectrum evolves continuously towards the strong-coupling limit. On the contrary, along the BCS line, a crossover is found between a regime, at low $|V|$, in which the minimum is at $2k_F$, and the strong coupling regime for which the minimum is at $4k_F$. We will see hereafter that a similar crossover is found in the density fluctuations and Friedel oscillations. Lastly, one can note that the sound velocity $u$ slowly decreases through this crossover line (and slower than on the SU(4) line), again in agreement with the perturbative prediction.

### 3.4 Quartets formation on the SU(4) line

In this section, we discuss the crossover from the weak-coupling regime to the strong-coupling regime on the SU(4) line as the attractive interaction is increased. When $|U|$ is large, the physics is essentially the one of hard-core bosons with repulsive interactions, as it has been discussed in Section 2.1 within the low-energy approach. To investigate how the quartets form, we can compute the local density of these "molecules". From a more general point of view, and to compare with the SU(2) case, we consider $N$-particle bound states in the context of the SU($N$) Hubbard model [26]. The local density of molecules is $m(x) = \langle n_{x,1} \dots n_{x,N} \rangle$ (which we denote by $q(x)$ for quartets). For free fermions, this operator has a finite expectation value that we subtract to keep only the connected part $m(x) = \langle n_{x,1} \dots n_{x,N} \rangle - (n/N)^N$. If molecules are tightly bound on-site, we expect $\langle n_{x,1} \dots n_{x,N} \rangle$ to be close to $n/N$ though slightly lower. Therefore, we can define a molecule fraction (number between zero and one) as

$$\%\text{Molecules} = \frac{\overline{m(x)} - (n/N)^N}{n/N - (n/N)^N}, \qquad (12)$$

where the bar means averaging over all sites. The evolution of this quantity along the SU(2) and SU(4) lines are compared in Figure 7 as a function of $NU$ (and not $U$) because the interaction term scales like $N^2$ while the kinetic term only scales as $N$. At large $|U|$, molecules are tightly bound, but the SU(4) model is closer to a hard-core boson model than the SU(2) one. Another difference is the low-$U$ increase which is linear for SU(2) and power-law for SU(4) with an exponent larger than 2. Note that the behavior should also depend on density, particularly at small $U$.

Consequently, we expect the large negative $U$ physics to be essentially the one of hard-core boson. Still, we emphasize a major difference between SU(2) and SU(4): from perturbation theory, the SU(2) case leads to hard-core bosons with equal effective hopping and nearest-neighbor repulsion (also equivalent to an effective spin-1/2 XXZ chain [63]); on the contrary, in the SU($N$) case (with $N > 2$), the effective hopping at $N^{\text{th}}$ order in perturbation theory behaves as $t^N/|U|^{N-1}$, so it is negligible compared to nearest-neighbor repulsion, which is of order $t^2/|U|$.

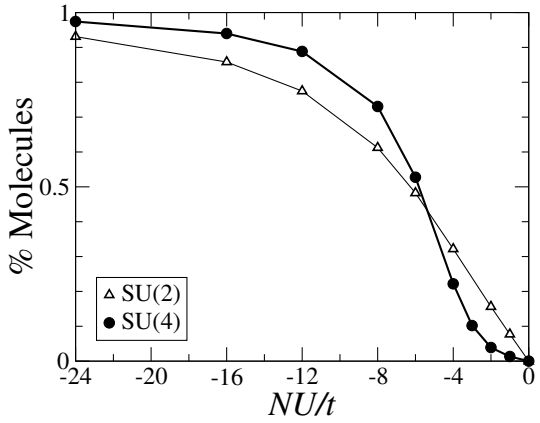


**Fig. 7.** Fraction of molecules in the system as a function of $U$ for the SU(2) and SU(4) models as defined by equation (12) from a system with $L = 64$ and density $n = 1$.

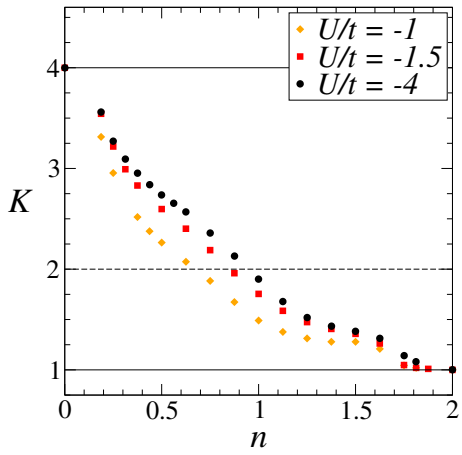


**Fig. 8.** (Color online) Luttinger parameter $K$ vs. filling $n$ for various $U$ obtained by fitting quartet correlations as in Figure 1 for the SU(4) model. $K \to 4$ when $n \to 0$ and $K \to 1$ when $n \to 2$ are the asymptotic behavior of the strong-coupling limit.

### 3.5 Evolution of the Luttinger parameter and the commensurate phase ADW$^\pi$ for n = 2

The previous considerations allow for a simple interpretation of the behavior of the Luttinger parameter $K$ as a function of the density $n$ for large negative $U$. DMRG results are given in Figure 8. As expected from the strong coupling argument, $K$ decreases from $K = N$ to $K = N/4$ (from 4 to 1) as the density $n$ varies from 0 to half-filling ($n = 2$). Particle-hole symmetry would give the behavior for $2 \leq n \leq 4$. Again, we recall that molecular superfluidity is the dominant instability when $K > 2$, which is generically the case at low enough density. When $n = 2$, a fully gapped phase is obtained with short-range quartet correlations. The phase is two-fold degenerate with a $\pi$ ordering of the local density (one quartet every two sites). Hence, we call this phase ADW$^\pi$. In terms of an effective bosonic model discussed in the previous paragraph, this corresponds to a "charge" density wave phase of the equivalent bosonic model at half-filling [64,65]. The density of bosons being 1/2, the corresponding critical value

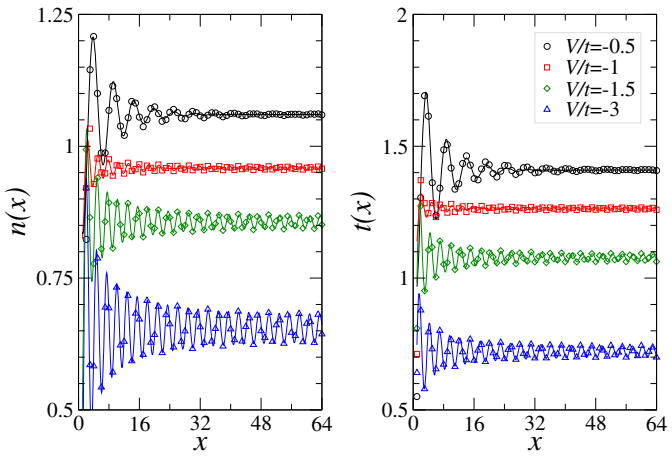


**Fig. 9.** Local density $n(x)$ and kinetic energy $t(x)$ along the BCS line at filling $n = 0.75$ on a $L = 128$ chain for increasing $|V|$. Friedel oscillations of the density have been shifted vertically for clarity. Thin lines are fits to results from DMRG calculations (see text).

for their Luttinger parameter [52] is $K_b = 1/2$ (at fixed density, changing interactions), which gives $K = 2$ for our model. As $K = 1 < 2$, the ADW$^\pi$ phase emerges as soon as the interaction $U$ is turned on. Working at fixed interactions and varying the density, the critical value is now $K_b = 1/4$, which gives the observed limiting value $K = 1$ as one approaches $n = 2$ (see also Ref. [26]).

### 3.6 Density fluctuations and Friedel oscillations

The density fluctuations can be analyzed from the correlations structure factor $N(k)$ with QMC, and from the behavior of the Friedel oscillations of the local density in open chains, as usually done in DMRG. The Friedel oscillations are the response of the fermionic density to the open end of the chain, which acts as an impurity. These modulations can give access to Luttinger parameters [66]. Data for the SU(4) line (not shown), and more generally in the ADW/MS region of the phase diagram, are all consistent with the low-energy predictions [14,15,43] $N(x) \sim \cos(2k_F x)x^{-K/2}$ for the density correlations and $n(x) \sim \cos(2k_F x)x^{-K/4}$ for the Friedel oscillations. Note that the $N(2k_F)$ peak diverges with the system size $L$ provided $K < 2$, signaling the quasi-ordering of the density fluctuations of the ADW phase [43].

Friedel oscillations in the BCS phase have a different behavior. As shown in Figure 9 for the generic density $n = 0.75$, there is a qualitative change in the wave-vector of the oscillations from $2k_F$ at low $|V|$ to $4k_F$ at large $|V|$. The predictions are that the $2k_F$ term should be short-range but a $4k_F$ term can develop with correlations $N(x) \sim \cos(4k_F x)x^{-2K}$. For the Friedel oscillations, we thus expect a leading contribution behaving as $n(x) \sim \cos(4k_F x)x^{-K}$, similar to what was found in two-leg ladders [67]. To explain the behavior observed in Figure 9, we argue that at low $|V|$, the amplitude of the $2k_F$ term remains significant (it is finite for a free system at $V = 0$) and with a correlation length which is still large (see Fig. 5). When $|V|$ increases, the $4k_F$ term emerges with an increasing amplitude. Fits have been carried out in Figure 9 using $n(x) = n_0 + n_1 \cos(2k_F x + \delta)e^{-x/\xi}$ for $V/t = -0.5$ and $n(x) = n_0 + n_1 \cos(4k_F x + \delta)/[d(x|L)]^K$ for larger $|V|$. The Luttinger exponents obtained from the fits are close to the ones obtained from the pairing correlations. In addition to DMRG calculations, DQMC data (see for instance Fig. 4 of Ref. [43] and other results not shown) support a similar qualitative change in the wave-vector and no divergence of the $4k_F$ amplitude with the system size. Indeed, this divergence only occurs for $K < 1/2$, i.e. in the MDW phase. Lastly, the same crossover around $V/t = -1$ is found in Figure 6b.

The crossover to the large $|V|$ physics can be qualitatively understood within the following picture: when $V$ is large, Cooper pairs have a tendency to form on-site, and certainly repel each other to gain local kinetic energy. This gives a typical $4k_F$ fluctuation of the local density and kinetic energy as found in Figure 9. The local kinetic energy term is $t(x) = \langle \sum_\sigma c^\dagger_{x+1\sigma} c_{x\sigma} \rangle$. In the ADW/MS region, it follows the Friedel oscillations of the density, so we have $t(x) \sim \cos(2k_F x)x^{-K/4}$. In the BCS/MDW region, the $2k_F$ component is short-range so the leading term is the $4k_F$ one, $t(x) \sim \cos(4k_F x)x^{-K}$, as for $n(x)$. The enhancement of these fluctuations (the total kinetic energy rather decreases with interactions as seen in Fig. 9) as $|V|$ is increased is reflected through the decrease of the Luttinger exponent $K$, as it was found for $n = 1$ in Figure 5 of reference [43]. A similar slow decrease with values of $K$ lower than one at large $|V|$ is found for $n = 0.75$. This decrease is not predicted in the perturbative estimate of equation (3) and is therefore a typical strong-coupling behavior. If one adds the repulsive interaction $U$ on-site, strictly on-site pairs are no more favored and the pairs lower their energy by delocalizing themselves on a bond. If $U$ is large enough and the density commensurate at $n = 1$, this qualitative picture leads to the bond-order wave phase observed in Figure 7 of reference [43] which breaks translational symmetry and is two-fold degenerate.

### 3.7 The transition between BCS/MDW and ADW/MS

This section gives some results on the transition line between the two regions BCS/MDW and ADW/MS. It was already shown that it belongs to the Ising universality class and that the ratio between the pairing and quartet correlations $R(x) = P^4(x)/Q(x)$ has the universal behavior $1/x$ at the critical point in agreement with conformal field theory (CFT) predictions [15,31,43].

#### 3.7.1 Effect of the density on the transition line

We first investigate the question of the dependence of the transition line with respect to the density $n$. This is an important issue for inhomogeneous systems, such as trapped cold atoms, since the local density in the cloud evolves continuously from zero to a finite value in the bulk. We

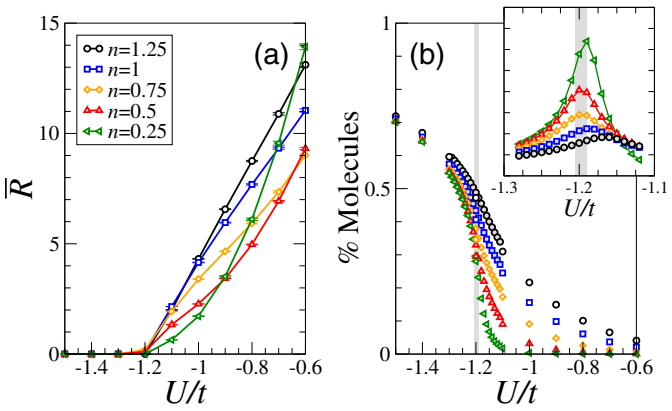


**Fig. 10.** Effect of the density on the transition line with fixed $V/t = -2$. (a) Averaged ratio $\overline{R}$ signaling the BCS/MS transition for different densities. The critical point $U/t \simeq -1.2$ of the BCS/MS transition hardly depends on density, even in the strong coupling limit. (b) The fraction of molecules (quartets) does not give a direct estimate of the transition but its derivative (inset) does. Open symbols are for a system with $L = 128$ while symbols filled with grey correspond to $L = 32$ (finite size effects are stronger at large density but remain small).

know that the perturbative result $U = V$ for this line does not depend on $n$, while the crossover lines in Figure 3 noticeably depend on $n$ from equation (3). In the strong coupling regime, we study numerically the transition line for several densities. To that purpose, we first use the behavior of $R(x)$ averaged over distances ranging from $x = 20$ to 40 (from correlations in a system with $L = 128$), which we denote by $\overline{R}$. In reference [43], the same ratio was used for a fixed distance $x = 45$ for $n = 1$; the two procedures lead to the same results but the first one is more suited to systems with low densities as oscillations have a longer wave-length. From Figure 10a, we see that $\overline{R}$ vanishes linearly around the critical point which is due to the Ising nature of the transition [43]. However, the higher the density, the wider the range of $U$ over which the linear behavior is observed. At density $n = 0.25$, the linear behavior is not recovered, certainly because of our mesh points. The main result is that the position of the critical point $U/t \simeq -1.2$ hardly depends on the density, though corresponding to the strong coupling regime.

Experimentally, it would be impossible to measure $\overline{R}$ so it is interesting to look at the behavior of the molecule fraction through the transition. This is given in Figure 10b in which one finds that the molecule fraction increases from the BCS/MDW to the ADW/Ms region, but rather smoothly at large densities. However, taking the derivative of the curve with respect to $U$ gives a clear peak pointing at the critical point. Consequently, this would be a rather simple way to locate the transition line experimentally as it could be measured and works even for an inhomogeneous cloud. The dependence of the peak with respect to the density is found to be small.

### 3.7.2 Entanglement entropy and central charge

Another prediction from CFT concerns the behavior of the central charge $c$ of the model at the transition line. The central charge somehow measures the effective Ising degrees of freedom in the low-energy physics. It is expected to be one in both regions (one gapless bosonic modes) around the transition but exactly equal to 3/2 at the transition due to the emergence of the Ising criticality with central charge $c = 1/2$. A simple way to extract the central charge with DMRG is to use the behavior of the von Neumann entanglement entropy $S_{vN}(x)$ of a block of size $x < L$. It is defined as

$$S_{vN}(x) = -\mathrm{Tr}[\rho(x) \ln \rho(x)], \qquad (13)$$

where $\rho(x)$ is the reduced density matrix of the block. As has been emphasized recently in several studies, the use of the entanglement entropy can provide crucial information for condensed matter studies since it allows to detect quantum phase transitions without any knowledge on the order parameters [68]. It is straightforwardly computed with the DMRG algorithm from the eigenvalues of the reduced density matrix which is obtained at each iteration. Following the ideas developed in references [69,70], a subleading oscillating term emerges due to open boundary conditions. Similarly to what happens in the XXZ model, we expect the oscillations to be related to the local kinetic energy $t(x)$ (similar to the dimerization term). Indeed, we can carry out fits in both regions by using the following ansatz

$$S_{vN}(x) = \frac{c}{6} \ln d(x|L) + A + B(t(x) - \overline{t}), \qquad (14)$$

where $\overline{t}$ is the mean value of $t(x)$ in the bulk, and $A, B$ are two constants. The behavior of the entanglement entropy thus gives access to the central charge $c$. In Figure 11, a clear jump of $c$ is observed at the transition. The expected value $c = 1$ is well reproduced in the two regions away from the critical point. At the transition, the fit is not as accurate but restricting it to the bulk region yields $c = 1.51$, at the price of describing less well the strong oscillations close to the edges (a fit including all data yields $c = 1.71$ but overestimates the behavior in the bulk). Note that the singular behavior of $c$ differs from the continuous behavior of $K$ and the gaps at the transition. Note also that the $2k_F$ oscillations in the ADW/MS region are reminiscent of similar features seen in local density and kinetic energy, and compatible with a $2k_F$ soft mode (see Fig. 6a) [71]. A last remark is that the local kinetic energy oscillations on the transition line should follow $t(x) \sim \cos(2k_F x) x^{-(K+1)/4}$, i.e. an exponent between those in the neighboring BCS/MDW region (provided $K > 1/3$) and ADW/MS region.

## 4 Experimental signatures of MS phase

This section is devoted to the study of effects particularly relevant for experimental set-ups. In addition to these results, we have already discussed in Section 3.3 the excitation gaps, relevant for radio frequency spectroscopy, and

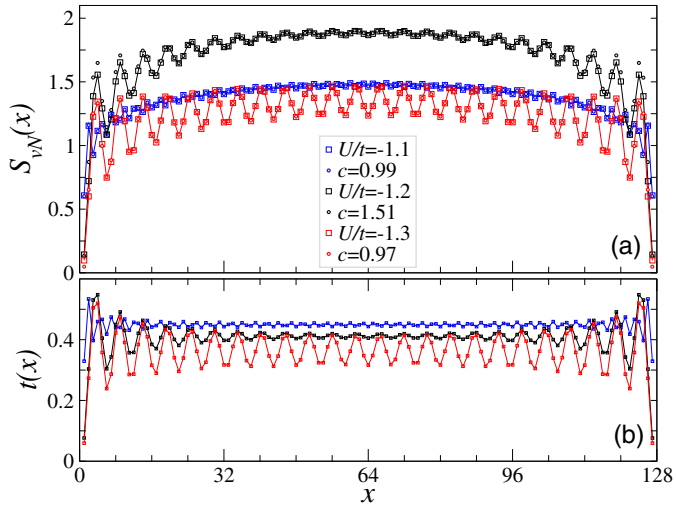


**Fig. 11.** Von Neumann block entropy $S_{vN}(x)$ for a block of size $x$ and local kinetic energy $t(x)$ around the critical point $U/t = -1.2$ for fixed $V/t = -2$ and $n = 0.75$ (see Fig. 10) with $L = 128$. Fits (filled circles) using equation (14) are quite accurate, allowing for the determination of the central charge $c$.

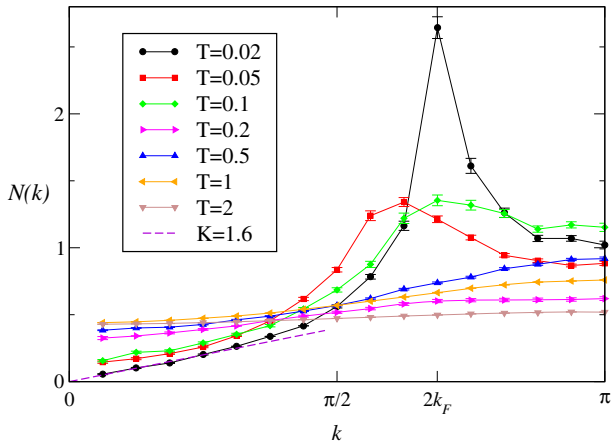


**Fig. 12.** SU(4) model: $N(k)$ obtained from QMC SSE simulations at various temperatures (in units of $t$) for $U/t = -2$, $L = 32$ and $\mu = -3.4t$. At low temperature, the small-$k$ linear behavior allows to extract $K \simeq 1.6$ which is compatible with DMRG estimate of 1.5 for same parameters. Moreover, the temperature effect allows to estimate at which energy scale the $2k_F$ peak appears. $k_F$ shown on the plot corresponds to the mean density $\langle n \rangle = 1.4$.

the molecule fraction, which could be measured experimentally from pictures resolving the hyperfine states.

### 4.1 Effect of temperature on the $2k_F$ peak

Using QMC, it is possible to investigate the energy scale at which the zero-temperature features become relevant. In Figure 12, we study the effect of temperature on the density structure factor $N(k)$ calculated on the SU(4) line for different temperatures. Let us remind that we work in a grand-canonical ensemble so that the density $\langle n \rangle$ varies with temperature (typically between 1.2 and 1.6 for this plot). In particular, we have shown the $2k_F$ location corresponding to the low-temperature density ($\langle n \rangle = 1.4$). The two properties of interest are the emergence of the $2k_F$ peak, and the linear behavior at small-$k$. We observe that, below a typical temperature of order $0.1t$, these two features qualitatively approach their $T = 0$ behavior, while a quantitative estimate requires a much lower temperature of order $0.02t$. If these features could be measured experimentally, one could identify the two main regions from the strength of the $2k_F$ and $4k_F$ peaks.

### 4.2 Effect of the trap

The effect of the trap confinement on two-component fermionic gases loaded in optical lattices has been studied for repulsive [72] and attractive [63,73] interactions. Trapped fermions with attractive interactions were also studied for imbalanced populations [74], i.e. with no SU(2) symmetry. The Hamiltonian term corresponding to the harmonic confinement is:

$$\frac{\omega^2}{2} \sum_i (i - (L+1)/2)^2 n_i, \tag{15}$$

with $\omega$ the trap frequency and $(L+1)/2$ the middle of the chain. We thus take the box width $L$ to be larger than the cloud's width not to induce boundary effect from the edges of the box. Without a lattice, the chemical potential reads $\mu = \omega N_f/N$ for free fermions. The thermodynamical limit is understood as taking the $\omega \to 0$ limit while keeping $N_f\omega$ constant so that the density at the center of the trap remains constant. Consequently, $N_f\omega$ is similar to an effective density of the system and, depending on it, several regimes are identified.

The density profile of the condensate $n(x)$ (or $n_i = n(x_i)$ in case of a lattice) is directly accessible from experimental pictures. For free fermions without an optical lattice in the Tonks-Girardeau (TG) regime with $N$-color [75–77], one has

$$n_{TG}(x) = n_0 \sqrt{1 - x^2/R_{TG}^2} \tag{16}$$

with $R_{TG} \sim \sqrt{N_f/N\omega}$ and $n_0 \sim \sqrt{N_f\omega/N}$, on which we observe that $n_0$ is kept constant in the thermodynamical limit. These results are valid if the trap evolves smoothly enough such that the local density approximation (LDA) is expected to be a reasonable assumption. In presence of an optical lattice, the energy per particle and the dispersion relations are changed. In this situation, LDA gives a density profile of the type $n(x) = n_0 \arccos(x^2/R^2 - b^2)/\arccos(-b^2)$ for $|x| \leq R\sqrt{1+b^2}$ [78]. The typical width of the density distribution, which can be measured, is defined as $W = 2\sqrt{\frac{1}{N_f}\sum_i (i - i_0)^2 n_i}$. In the Tonks-Girardeau regime, we have $W \sim R_{TG} \sim \sqrt{N_f/N\omega}$, so that $W \sim \omega^{-1}$ in the thermodynamical limit. We found a similar behavior for the spin-3/2 fermion model under study with a scaling which agrees well with the TG one, as one can infer from the results of Figure 13.

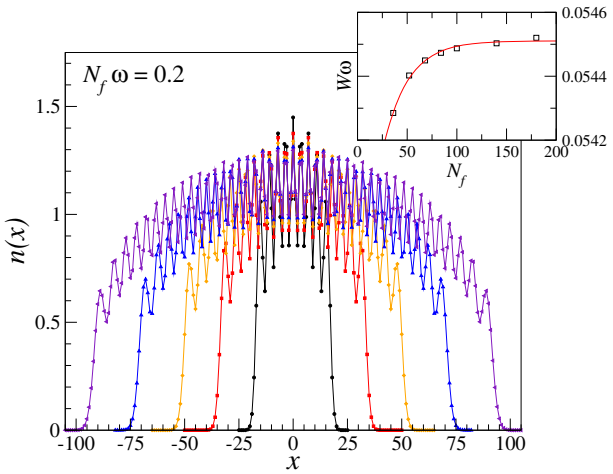


**Fig. 13.** Typical density profiles of the trapped condensate for fixed "density" $N_f\omega = 0.2$ and $U/t = -4$, with respectively $N_f = 36, 68, 100, 140, 180$. The inset shows the scaling of $W\omega$ in the thermodynamical limit, which well agrees with the TG behavior.

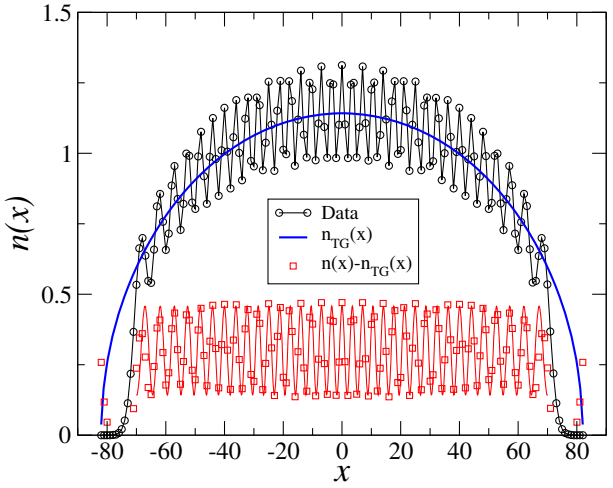


**Fig. 14.** Typical density profile of the trapped condensate on the SU(4) line ($U/t = -4$) with a smooth trap ($N_f\omega = 0.2$ and $N_f = 140$). One observes that $2k_F \simeq \pi/2$ oscillations develop at the center of the cloud. Close to the edges, the wave-length of the oscillations increases, qualitatively following the local decrease of the local averaged density. A reasonable fit for the bulk physics is obtained using the Tonks-Girardeau result plus an oscillating term.

### 4.2.1 Atomic density waves

For sufficiently smooth traps, the bulk of the condensate features the typical $2k_F$ oscillations reminiscent of the ADW phase encountered with open-boundary conditions. For instance, Figure 14 shows a typical density profile on the SU(4) line. The density profile can be reasonably fitted up to the edges by a Tonks-Girardeau profile (Eq. (16)) plus an oscillating term

$$n(x) = n_{TG}(x) + \delta n \cos(2\tilde{k}_F(x)x), \tag{17}$$

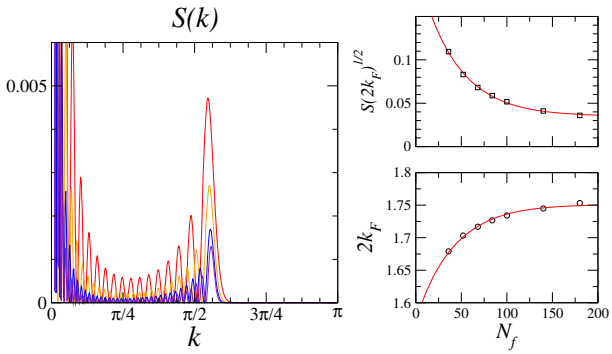


**Fig. 15.** The density structure factor $S(k)$ corresponding to Figure 13 (same color code), and the scaling of the $2k_F$ peak position and amplitude in the thermodynamical limit.

with the effective Fermi wave-vector

$$\tilde{k}_F(x) = \frac{\pi}{4} n_0 \sqrt{1 - x^2/(\tilde{R}_{TG})^2}. \tag{18}$$

In Figure 14, we first fit the TG profile and subtract it from the data to only keep the oscillating term that we fit using the same value of $n_0$. The slight dependence of $\tilde{k}_F$ on $x$ accounts for the increase of the wave-length as the density decreases towards the edges of the condensate. However, if $\tilde{R}_{TG}$ is a free parameter of the fit, we find that $\tilde{R}_{TG} \simeq 2R_{TG}$ gives a better fit of the oscillations. This discrepancy could be due to finite size effects, as the TG profile should be valid for large enough systems and far enough from the edges of the condensate. The condensate has sharp edges (LDA usually fails to explain the behavior close to the edges) and in the following, we call $a$ the radius at which the density vanishes ($a \lesssim R_{TG}$).

The main question is now to discuss the thermodynamical limit of the oscillations amplitude in the bulk $\delta n$. For non-trapped gases in a box, we expect the oscillations to be zero in the middle of the system (except for a translationally breaking phase) as the Friedel oscillations decay away from the boundaries. In the SU(2) case, a finite $\delta n$ has been found around the commensurate density $n_0 = 1$ [63,73]. These atomic-density waves will have clear signatures in the density structure factor that can be measured with light-scattering diffraction. The latter is defined by

$$S(k) = \left| \frac{1}{N_f} \sum_j e^{ikj} n_j \right|^2, \tag{19}$$

and an example is given in Figure 15. The main features of the structure factor is the peak at $2k_F \simeq \pi n_0/2$ which signals the ADW oscillations of the trapped systems. Oscillations in $S(k)$ are due to the finite size $2a$ of the condensate and may vanish for large systems. We expect the height of the peak to be proportional to $(\delta n)^2$ for large enough systems. The insets of Figure 15 show the evolution of $\sqrt{S(2k_F)} \sim \delta n$ and $2k_F$ (defined as the $k$ at which the peak has its maximum) as a function of $N_f$. Fits are obtained for both quantities with an exponential law $s_0 + s_1 e^{-N_f/\xi}$. We infer from these results that

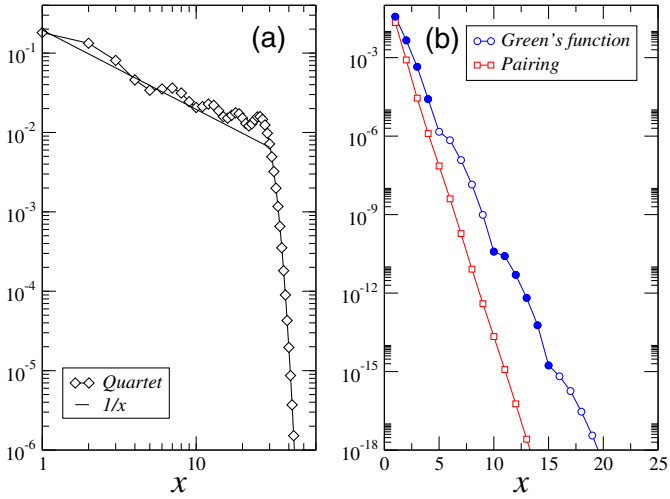


**Fig. 16.** Correlations in a trap system with $\omega = 0.002$, $U = -4$, $V = 0$ and $N_f = 36$. (a) Quartet correlations $Q(x)$ showing dominant MS correlations (from comparison with $1/x$). (b) Pairing and Green's function are short-range. The full (open) circles account for the $+(-)$ sign coming from the $\sin(k_F x)$ term.

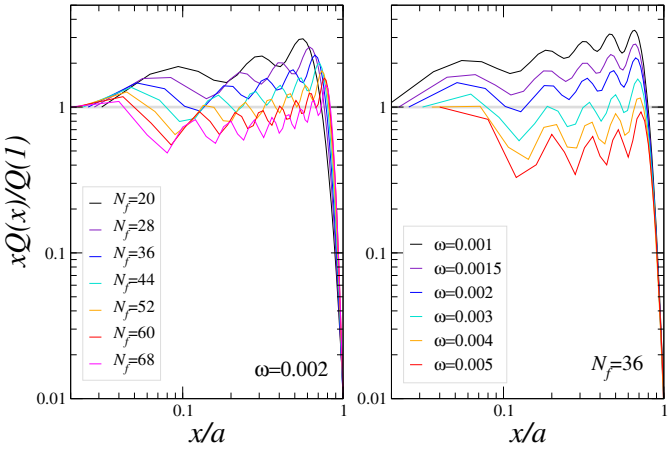


**Fig. 17.** (a) Correlations in a trapped system with $U = -4$ and $V = 0$ (a) for fixed $\omega = 0.002$ and various $N_f$. The distance $x$ is rescaled by the trap radius $a$. (b) The same for fixed $N_f = 36$ and varying $\omega$.

$\delta n$ is finite in the thermodynamical limit for our choice of parameters, similarly to what was found in the SU(2) case [63].

### 4.2.2 Correlations and the BCS/ADW transition

We now turn to the behavior of the correlations in trapped gases. They are computed by fixing one point of the correlator at the center of the cloud and letting the position $x$ of the other ranging from the middle to the edge of the condensate. For a trapped condensate, a gap computed from energy differences can be spoiled by edges effect. To check the gapped nature of the one- and two-particle excitations along the SU(4) line, we compute the Green's function and the pairing correlation. From the behavior of the quartet correlations, we can deduce the leading fluctuations in the bulk of the cloud. These results are given in Figure 16 in which we see that for this small value of the effective density ($N_f\omega = 0.07$), the physics in the bulk is essentially the same as for the non-trapped system. Quartet correlations slightly increase as one approaches the edge of the condensate. Assuming the LDA approximation to work in such small systems, we expect the local Luttinger parameter [79,80] controlling the power-law decrease of the correlations $K(x) = K(n(x))$ to increase with decreasing densities, following the homogeneous system result of Figure 8. As the quartet correlations behave as $2/K$ and because $K$ decreases with density, they are actually reinforced by the harmonic confinement. Trapping thus favors the observation of the MS phase. By lowering the effective density $N_f\omega$, we expect a crossover from subleading to leading quartet correlations. In Figure 17, we show both the effect of changing the number of particles $N_f$ while keeping $\omega$ constant and the opposite situation where $\omega$ varies. We find that quartet correlations always decreases slower than $1/x$ (corresponding to the critical value $K_c = 2$) below approximately $N_f\omega \simeq 0.08$.

### 4.2.3 Effect of varying interactions and deep trap physics

In this section, we address the question of the effect of varying interactions on the density profile of the condensate. We expect the width of the condensate to strongly depend on interactions: repulsive interactions make the condensate inflate while attractive interactions can strongly reduce $W$. In the large trap frequency limit, we furthermore have a minimal width of the condensate due to Pauli's exclusion principle which depends on the number of colors: $W^{min} = \sqrt{\frac{1}{3}\left((N_f/N)^2 - 1\right)} \sim N_f/\sqrt{3}N$. Thus, starting from free electrons and keeping $N_f\omega/N$ constant, the ratio $W^{min}/W^{free} \sim \sqrt{N_f\omega/N}$ should be constant. We give a comparison with the evolution of the width in the SU(2) case as a function of $NU$: the collapse of the condensate is faster in the SU(4) case. In Figure 18, we show, for a constant and rather large effective density $N_f\omega = 1.4$, the evolution of the condensate when increasing (negative) $U$ along the SU(4) line. Two effects are observed: the width of the condensate strongly decreases which induces a sharp increase of the density at the center of the trap. Consequently, the effective Fermi wave-vector increases, which can be observed in the density structure factor. Similar effects have been found for the SU(2) attractive model [81,82]. Because the effective density is large enough, the commensurate ADW$^\pi$ phase develops when $n_0 \geq 2$. A strong signal at $k = \pi$ is then present in the density structure factor.

Moving away from the SU(4) line, we can investigate the behavior of the density profile across the transition between the two regions of the phase diagram of Figure 3. Indeed, we have seen in Section 3.7.1 that the transition line hardly depends on the density. Therefore, for inhomogeneous density profiles, we expect the transition to hold

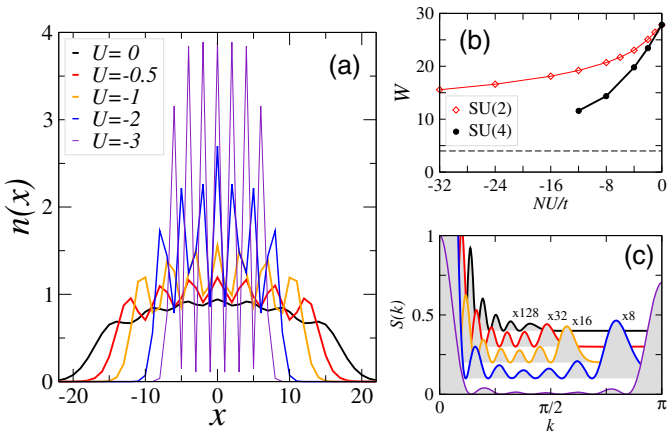


**Fig. 18.** (a) Typical density profiles of the trapped condensate for various interaction strength $U$ on the SU(4) line. There are $N_f = 28$ fermions and $\omega = 0.05$. (b) Width of the condensate as a function of $U/t$. Its width is roughly divided by a factor 2.5. The SU(2) line has been computed with the same $\omega$ but with 14 fermions. The width is much more sensitive to $U$ in the SU(4) case. (c) Structure factors have been rescaled for clarity.

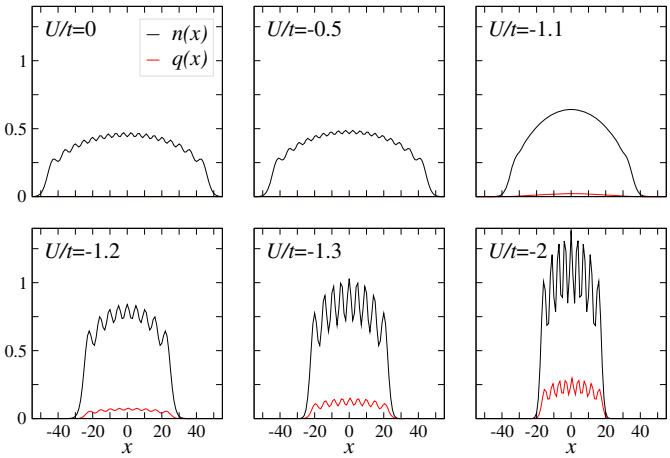


**Fig. 19.** Evolution of the profiles along the $V = -2$ line with decreasing $U$ showing the crossing of the transition (located at $U/t = -1.2$).

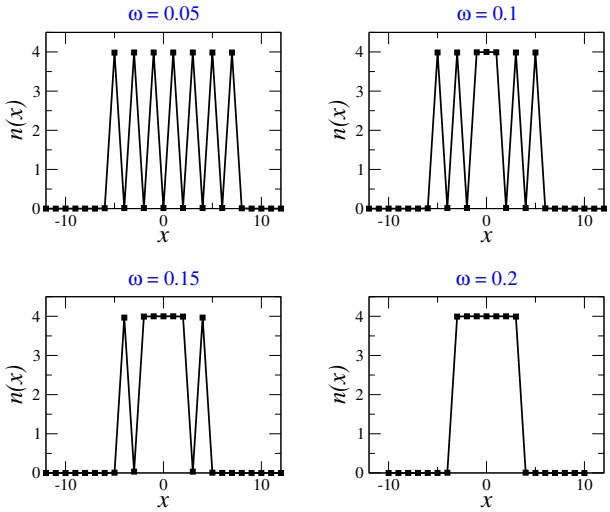


**Fig. 20.** Starting with a system with strongly bound quartets ($N_f = 28$, $U/t = -8$), one can increase the frequency of the trap. Quartets have a tendency to repel each other but when the trap is too deep, they progressively melt at the center of the trap.

for identical parameters, and that the whole cloud will be affected by the phase transition (meaning that no domains will form). Note that this is not true for the crossover lines inside each region of Figure 3, and that is seen through the variation of $K(n(x))$ in Figure 17. The typical evolution of $n(x)$ along the $V/t = -2$ line (varying $U$) is given in Figure 19. Two main effects are visible: the width of the condensate is roughly divided by two, and the amplitude of the Friedel like oscillations are strongly enhanced in the bulk. Remarkably, because of the strong increase of the density at the center of the cloud in the ADW/MS region, the wave-vector of the oscillations hardly changes (it is $4\tilde{k}_F$ in the BCS phase, but $2\tilde{k}_F$ in the ADW/MS region). If one is able to measure the local density of molecules, a crossover from zero to a significant value will be also observed across the transition, similarly to what was found in Figure 10. The fact that the density of quartets is spread over the whole condensate through the transition line supports the absence of domain formation.

If the trap is very deep, corresponding to large values of the effective density $N_f\omega$, all atoms will form an homogeneous condensate in the middle of the trap, the width of which is $W^{min}$ as discussed above. As displayed in Figure 20, this state emerges from the melting of the ADW$^\pi$ phase which can be qualitatively understood as the mere competition between the effective nearest neighbor repulsion of the quartets and the potential energy of the trap. This effect is very similar to the one found for the SU(2) model in reference [82]. For $\omega = 0.05$, the density profile is shifted from the center of the trap. Actually, the energy of such a shifted state is much smaller than other energy scales (equal to $0.00875t$ within a classical approximation), so that it is nearly degenerate to the ground-state and DMRG gets locked into it because the effective hopping term of the molecules is too small (for large $|U|$).

### 4.3 Flux quantization

In standard electronic systems, flux quantization experiments can directly measure the electric charge of the carriers by considering a *ring* geometry threaded by a magnetic flux and look at the flux periodicity of the total energy. In the case of neutral cold atoms, such a flux analogy could be realized thanks to the possibility of rotating the trap. Therefore, it could be possible to prove the existence of $N$ particle bound states by checking if minima of the energy are degenerate [15]. Moreover, ring-shape geometries have been realized experimentally [83–85] so that such experiments could be performed in the near future.

We have performed exact diagonalization for the SU(4) case on small chains of length $L = 8$. Although these sizes are relatively small, we expect that bound-state formation can already be checked since it is a local process. Indeed, as

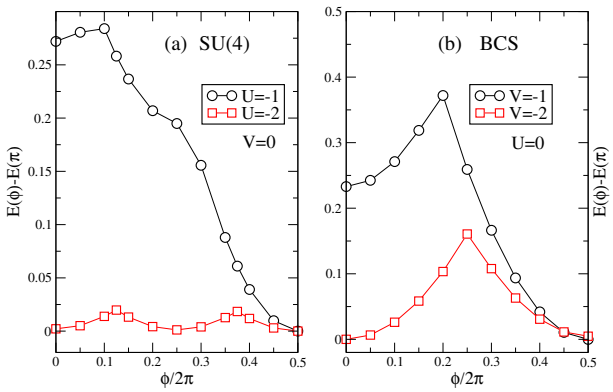


**Fig. 21.** Energy vs. flux for a periodic chain of length $L = 8$ with 8 particles for various interactions. Energies are measured relative to the absolute ground-state energy (here at $\phi = \pi$). (a) SU(4) model showing the appearance of 4 minima; (b) BCS phase with 2 minima. Note that only flux between 0 and $\pi$ are shown since data are symmetric $E(-\phi) = E(\phi)$ and $2\pi$ periodic.

the interaction strength increases, we see that the number of minima changes from one to four (see Fig. 21a) in the ADW/MS phase, while it increases from one to two in the BCS/MDW phase (see Fig. 21b), in full agreement with the predictions of the low-energy approach [15]. These observations are compatible with our predictions of four- and two-particle bound states, respectively. Note that the overall energy scales decrease since the band width is proportional to the effective molecular or pair hopping. Similar calculations suggesting pairing and superfluidity in a multicomponent fermionic model have been proposed recently [86]. As a final comment, let us remind the reader that the effect of such a flux corresponds to a twist in the boundary conditions, and therefore vanishes in the thermodynamic limit where $E(\phi)$ becomes flat. Still, such an effect can be observed on finite lattices.

## 5 Conclusion

Motivated by fermionic cold atoms experiments where generically many hyperfine states coexist, we have investigated spin 3/2 fermions with contact interactions in an optical lattice. We focus on the attractive case for a generic density. By using large-scale numerical techniques, we describe the phase diagram and discuss all competing phases. In particular, at low density, we confirm the existence of a large molecular superfluid phase where dominant correlations are superfluid-like made of four-particle bound-states. This phase has a large extension and is not restricted to the SU(4) model. In another region of the phase diagram, two-particle pairs become gapless, leading to a BCS phase. We have shown that the phase transition between MS and BCS phases can be located using entanglement measurements, such as the von Neumann entropy or the molecule fraction.

In order to make contact with possible experimental observations of such phases, we have investigated the role of the trapping potential. In many respects, correlations inside the bulk of the condensate are similar to the homogeneous case if the effective density is low enough. ADW oscillations can be probed from the density structure factor. Furthermore, we give an estimate for the crossover effective density below which leading MS fluctuations are dominant. Moreover, playing with the trap can provide useful informations about the size of the condensate and the density correlations, which are accessible experimentally. For instance, deep in the ADW/MS phase, the physics can be understood from tightly bound "molecules" that act as hardcore bosons. These objects could be measured either by looking at the molecule fraction or by using rf spectroscopy. Finally, we propose to distinguish between MS and BCS phase by using a ring-shape geometries. We hope that such experiments will be performed in the near future.

We would like to thank T. Barthel, E. Boulat, A.M. Läuchli, F. Heidrich-Meisner, P. Schuck, and S.R. White for useful discussions. G.R. and S.C. thank IDRIS (Orsay, France) and CALMIP (Toulouse, France) for use of supercomputers.

## References

1. M. Lewenstein, A. Sanpera, V. Ahufinger, B. Damski, A.S. De, U. Sen, Adv. Phys. **56**, 243 (2006)
2. M. Greiner, O. Mandel, T. Esslinger, T.W. Hänsch, I. Bloch, Nature **415**, 39 (2002)
3. R. Jördens, N. Strohmaier, K. Günter, H. Moritz, T. Esslinger, `arXiv:0804.4009`
4. I. Bloch, J. Dalibard, W. Zwerger, Rev. Mod. Phys. **80**, 885 (2008)
5. S. Giorgini, L.P. Pitaevskii, S. Stringari, to be published in Rev. Mod. Phys, `arXiv:0706.3360`
6. W. Ketterle, M.W. Zwierlein, to appear in *"Ultracold Fermi Gases", Proceedings of the International School of Physics "Enrico Fermi", Course CLXIV, Varenna, 20 - 30 June 2006*, edited by M. Inguscio, W. Ketterle, C. Salomon (IOS Press, Amsterdam, 2008), `arXiv:0801.2500`
7. D.S. Koltun, Phys. Rev. C **36**, 2047 (1987)
8. P. Schlottmann, J. Phys.: Condens. Matter **6**, 1359 (1994)
9. A.G.K. Modawi, A.J. Leggett, J. Low Temp. Phys. **109**, 625 (1997)
10. T.-L. Ho, S. Yip, Phys. Rev. Lett. **82**, 247 (1999)
11. A.S. Stepanenko, J.M.F. Gunn, `arXiv:cond-mat/9901317`
12. C. Honerkamp, W. Hofstetter, Phys. Rev. Lett. **92**, 170403 (2004)
13. C. Honerkamp, W. Hofstetter, Phys. Rev. B **70**, 094521 (2004)
14. C. Wu, Phys. Rev. Lett. **95**, 266404 (2005)
15. P. Lecheminant, E. Boulat, P. Azaria, Phys. Rev. Lett. **95**, 240402 (2005)
16. H. Kamei, K. Miyake, J. Phys. Soc. Jpn **74**, 1911 (2005)
17. T. Paananen, J.-P. Martikainen, P. Törmä, Phys. Rev. A **73**, 053606 (2006)
18. L. He, M. Jin, P. Zhuang, Phys. Rev. A **74**, 033604 (2006)
19. P.F. Bedaque, J.P. D'Incao, `arXiv:cond-mat/0602525`
20. A. Sedrakian, J.W. Clark, Phys. Rev. C **73**, 035803 (2006)
21. D. Lee, Phys. Rev. Lett. **98**, 182501 (2007)
22. Á. Rapp, G. Zaránd, C. Honerkamp, W. Hofstetter, Phys. Rev. Lett. **98**, 160405 (2007)

23. R.W. Cherng, G. Refael, E. Demler, Phys. Rev. Lett. **99**, 130406 (2007)
24. H. Zhai, Phys. Rev. A **75**, 031603 (2007)
25. T. Fukuhara, Y. Takasu, M. Kumakura, Y. Takahashi, Phys. Rev. Lett. **98**, 030401 (2007)
26. S. Capponi, G. Roux, P. Lecheminant, P. Azaria, E. Boulat, S.R. White, Phys. Rev. A **77**, 013624 (2008)
27. Á. Rapp, W. Hofstetter, G. Zaránd, Phys. Rev. B **77**, 144520 (2008)
28. D. Blume, S.T. Rittenhouse, J. von Stecher, C.H. Greene, Phys. Rev. A **77**, 033627 (2008)
29. X.-J. Liu, H. Hu, P.D. Drummond, Phys. Rev. A **77**, 013622 (2008)
30. X.W. Guan, M.T. Batchelor, C. Lee, H.-Q. Zhou, Phys. Rev. Lett. **100**, 200401 (2008)
31. P. Lecheminant, P. Azaria, E. Boulat, Nucl. Phys. B **798**, 443 (2008)
32. M. Bartenstein, A. Altmeyer, S. Riedl, R. Geursen, S. Jochim, C. Chin, J.H. Denschlag, R. Grimm, A. Simoni, E. Tiesinga, C.J. Williams, P.S. Julienne, Phys. Rev. Lett. **94**, 103201 (2005)
33. T.B. Ottenstein, T. Lompe, M. Kohnen, A.N. Wenz, S. Jochim, `arXiv:0806.0587`
34. B. DeMarco, Ph.D. thesis, University of Colorado, Boulder (2001)
35. G. Röpke, A. Schnell, P. Schuck, P. Nozières, Phys. Rev. Lett. **80**, 3177 (1998)
36. G. Röpke, P. Schuck, Mod. Phys. Lett. A **21**, 2513 (2006)
37. P. Nozières, D. Saint James, J. Phys. France **43**, 1133 (1982)
38. B. Douçot, J. Vidal, Phys. Rev. Lett. **88**, 227005 (2002)
39. M.-S. Chang, I. Affleck, Phys. Rev. B **76**, 054521 (2007)
40. T.-L. Ho, Phys. Rev. Lett. **81**, 742 (1998)
41. C. Wu, J.-P. Hu, S.-C. Zhang, Phys. Rev. Lett. **91**, 186402 (2003)
42. C. Wu, Mod. Phys. Lett. B **20**, 1707 (2006)
43. S. Capponi, G. Roux, P. Azaria, E. Boulat, P. Lecheminant, Phys. Rev. B **75**, 100503(R) (2007)
44. S.R. White, Phys. Rev. Lett. **69**, 2863 (1992)
45. S.R. White, Phys. Rev. B **48**, 10345 (1993)
46. U. Schollwöck, Rev. Mod. Phys. **77**, 259 (2005)
47. A.W. Sandvik, Phys. Rev. B **59**, R14157 (1999)
48. F. Alet, S. Wessel, M. Troyer, Phys. Rev. E **71**, 036706 (2005)
49. F.F. Assaad, *Quantum Monte Carlo Methods on Lattices: The Determinantal Approach* (John von Neumann Institute for Computing, Jülich, 2002), NIC Vol. 10, p. 99
50. D. Controzzi, A.M. Tsvelik, Phys. Rev. Lett. **96**, 097205 (2006)
51. A.O. Gogolin, A.A. Nersesyan, A.M. Tsvelik, *Bosonization and Strongly Correlated Systems* (Cambridge University Press, Cambridge, UK, 1998)
52. T. Giamarchi, *Quantum Physics in one Dimension*, International series of monographs on physics (Oxford University Press, Oxford, UK, 2004), Vol. 121
53. L. Kecke, T. Momoi, A. Furusaki, Phys. Rev. B **76**, 060407(R) (2007)
54. F.D.M. Haldane, Phys. Rev. Lett. **47**, 1840 (1981)
55. M.A. Cazalilla, J. Phys. B **37**, S1 (2004)
56. A.F. Albuquerque et al., J. Magn. Magn. Mater. **310**, 1187 (2007)
57. M. Troyer, B. Ammon, E. Heeb, Lect. Notes Comput. Sci. **1505**, 502 (1998)
58. S. Ejima, F. Gebhard, S. Nishimoto, Europhys. Lett. **70**, 492 (2005)
59. H.-H. Lin, L. Balents, M.P.A. Fisher, Phys. Rev. B **58**, 1794 (1998)
60. T. Giamarchi, B.S. Shastry, Phys. Rev. B **51**, 10915 (1995)
61. E. Orignac, T. Giamarchi, Phys. Rev. B **57**, 11713 (1998)
62. N. Andrei, J.H. Lowenstein, Phys. Lett. B **90**, 106 (1980)
63. G. Xianlong, M. Rizzi, M. Polini, R. Fazio, M.P. Tosi, J.V.L. Campo, K. Capelle, Phys. Rev. Lett. **98**, 030404 (2007)
64. J. Zhao, K. Ueda, X. Wang, Phys. Rev. B **74**, 233102 (2006)
65. J. Zhao, K. Ueda, X. Wang, J. Phys. Soc. Jpn **76**, 114711 (2007)
66. R. Egger, H. Grabert, Phys. Rev. Lett. **75**, 3505 (1995)
67. S.R. White, I. Affleck, D.J. Scalapino, Phys. Rev. B **65**, 165122 (2002)
68. L. Amico, R. Fazio, A. Osterloh, V. Vedral, Rev. Mod. Phys. **80**, 517 (2008)
69. N. Laflorencie, E.S. Sorensen, M.S. Chang, I. Affleck, Phys. Rev. Lett. **96**, 100603 (2006)
70. E.S. Sorensen, M.S. Chang, N. Laflorencie, I. Affleck, J. Stat. Mech., P08003 (2007)
71. O. Legeza, J.Sólyom, L. Tincani, R.M. Noack, Phys. Rev. Lett. **99**, 087203 (2007)
72. M. Rigol, A. Muramatsu, G.G. Batrouni, R.T. Scalettar, Phys. Rev. Lett. **91**, 130403 (2003)
73. R.A. Molina, J. Dukelsky, P. Schmitteckert, Phys. Rev. Lett. **99**, 080404 (2007)
74. A.E. Feiguin, F. Heidrich-Meisner, Phys. Rev. B **76**, 220508(R) (2007); M. Tezuka, M. Ueda, Phys. Rev. Lett. **100**, 110403 (2008); M. Rizzi, M. Polini, M.A. Cazalilla, M.R. Bakhtiari, M.P. Tosi, Rosario Fazio, Phys. Rev. B **77**, 245105 (2008); A. Lüscher, R.M. Noack, A.M. Läuchli, Phys. Rev. A **78**, 013637 (2008)
75. D.S. Petrov, G.V. Shlyapnikov, J.T.M. Walraven, Phys. Rev. Lett. **85**, 3745 (2000)
76. V. Dunjko, V. Lorent, M. Olshanii, Phys. Rev. Lett. **86**, 5413 (2001)
77. I.V. Tokatly, Phys. Rev. Lett. **93**, 090405 (2004)
78. B. Paredes, A. Widera, V. Murg, O. Mandel, S. Fölling, I. Cirac, G.V. Shlyapnikov, T.W. Hänsch, I. Bloch, Nature **429**, 277 (2004)
79. D.M. Gangardt, G.V. Shlyapnikov, Phys. Rev. Lett. **90**, 010401 (2003)
80. C. Kollath, U. Schollwöck, J. von Delft, W. Zwerger, Phys. Rev. A **69**, 031601 (2004)
81. M. Machida, S. Yamada, Y. Ohashi, H. Matsumoto, Phys. Rev. A **74**, 053621 (2006)
82. G. Xianlong, M. Polini, M.P. Tosi, V.L. Campo, V.L. Jr, K. Capelle, `arXiv:cond-mat/0506570`
83. J.A. Sauer, M.D. Barrett, M.S. Chapman, Phys. Rev. Lett. **87**, 270401 (2001)
84. W.H. Heathcote, E. Nugent, B.T. Sheard, C.J. Foot, New J. Phys. **10**, 043012 (2008)
85. C. Ryu, M.F. Andersen, P. Clade, V. Natarajan, K. Helmerson, W.D. Phillips, `arXiv:0709.0012`
86. T. Wang, J. Javanainen, S.F. Yelin, Phys. Rev. A **76**, 011601 (2007)